

Effect of bundling on the stability, equilibrium geometry, and electronic structure of $\text{Mo}_6\text{S}_{9-x}\text{I}_x$ nanowires

Seoung-Hun Kang,¹ Young-Kyun Kwon,^{1,*} and David Tománek^{1,2,†}¹Department of Physics and Research Institute for Basic Sciences, Kyung Hee University, Seoul 130-701, Korea²Physics and Astronomy Department, Michigan State University, East Lansing, Michigan 48824-2320, USA

(Received 13 August 2010; published 17 November 2010)

We use *ab initio* density-functional theory calculations to determine the effect of bundling on the equilibrium structure, electronic, and magnetic properties of $\text{Mo}_6\text{S}_{9-x}\text{I}_x$ nanowires with $x=0,3,4.5,6$. Each unit cell of these systems contains two S- and I-decorated Mo_6 clusters that are connected by S_3 linkages to form an ordered linear array. Due to the bistability of the sulfur linkages, the total energy of the nanowires exhibits typically many minima as a function of the wire length. We find the optimum interwire distance depends on composition and to a smaller degree on the orientation of the wires. Structural order is expected in bundles with $x=0$ and $x=6$, since there is no disorder in the decoration of the Mo clusters. In bundles with other stoichiometries we expect structural disorder to occur. We find that the electronic structure of some nanowires can be switched from metallic to semiconducting by changing the interwire separation. Also, we find that selected stable or metastable nanowire geometries exhibit ferromagnetic behavior.

DOI: 10.1103/PhysRevB.82.205427

PACS number(s): 81.05.Zx, 61.46.-w, 68.65.-k, 73.22.-f

I. INTRODUCTION

Molybdenum chalcogenide (MCH) nanowires (NWs) (Refs. 1 and 2) have emerged as unique nanoscale building blocks for a wide range of applications. They combine many useful properties such as a high Young's modulus³⁻⁵ and a wide range of electrical transport as well as magnetic properties.^{4,6-9} Nanomechanical studies indicate a very low shear modulus of the bundled nanowires,⁵ suggesting self-lubricating properties and potential applications in nanotribology.^{10,11}

Recent experimental^{2,5,11-19} and theoretical^{4,8,12,14} studies all agree that MCH NWs form bundles but disagree on the type and strength of the interwire interaction. Whereas all experimental data suggest that nanowire bundles are rather robust and hard to disperse, some calculations indicate a flat electronic band dispersion in the plane normal to the wire axis in the bundle, suggesting only weak van der Waals-type interactions.^{4,12,14} Those latter results, obtained at a fixed interwire distance without structural optimization, disagree with data indicating the presence of a strong anisotropic interwire interaction in selected systems that may modify the electronic structure.⁸

To provide insight into the effect of the interwire interaction on structural and electronic properties of $\text{Mo}_6\text{S}_{9-x}\text{I}_x$ nanowires, we performed a theoretical study of their equilibrium structure, bundling energy, and electronic properties in the full composition range $0 \leq x \leq 6$. We find that most nanowires undergo significant structural relaxations when forming bundles. The energy gain associated with these relaxations contributes significantly to an attractive interwire interaction and bundling energy. We report large changes in the band structure along the wire, augmented by onset of band dispersion normal to the wire following the bundle formation. Our study also reveals the occurrence of magnetic instabilities in selected local structural optima.

II. COMPUTATIONAL METHOD

To investigate the structural and electronic properties of $\text{Mo}_6\text{S}_{9-x}\text{I}_x$, we optimized the geometry of infinite free and

bundled $\text{Mo}_6\text{S}_{9-x}\text{I}_x$ nanowires under different constraints using *ab initio* calculations in the framework of the density-functional theory (DFT). We used the Perdew-Zunger form²⁰ of the Ceperley-Alder exchange-correlation functional²¹ in the local-density approximation to DFT, as implemented in the SIESTA code.²² The behavior of valence electrons was described by norm-conserving Troullier-Martins pseudopotentials²³ with partial core corrections in the Kleinman-Bylander factorized form.²⁴ An atomic orbital basis with a double- ζ polarization was used to expand the electronic wave functions. We complemented the Mo basis by including initially unoccupied $5p$ orbitals.

Our studies address both infinite isolated nanowires with different stoichiometries and their bundled counterparts, depicted in Figs. 1(a) and 2(a). All systems are described by a periodic arrangement of unit cells with axial lattice constant a containing 30 atoms in 2 formula units of the $\text{Mo}_6\text{S}_{9-x}\text{I}_x$ compound.

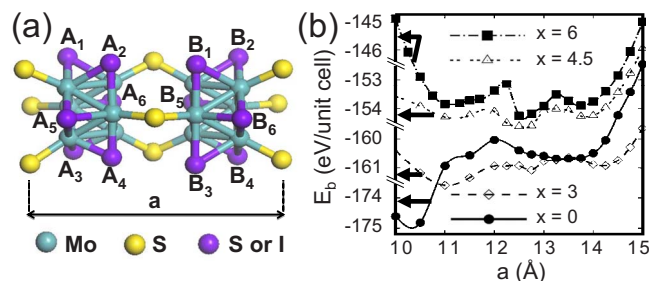


FIG. 1. (Color online) (a) Atomic arrangement within an isolated $\text{Mo}_6\text{S}_{9-x}\text{I}_x$ nanowire. The unit cell of length a contains 2 formula units, including 12 Mo atoms arranged in two octahedra. The S_3 linkages connecting the Mo_6 octahedra are shown at both ends of the unit cell. Sites decorating the Mo octahedra are denoted by A_i and B_i and may be occupied by either S or I atoms. (b) Binding energy per unit cell as a function of the lattice constant a for different iodine concentrations x . For better visualization of energy differences within each stoichiometry, the energy axis has been split into four segments.

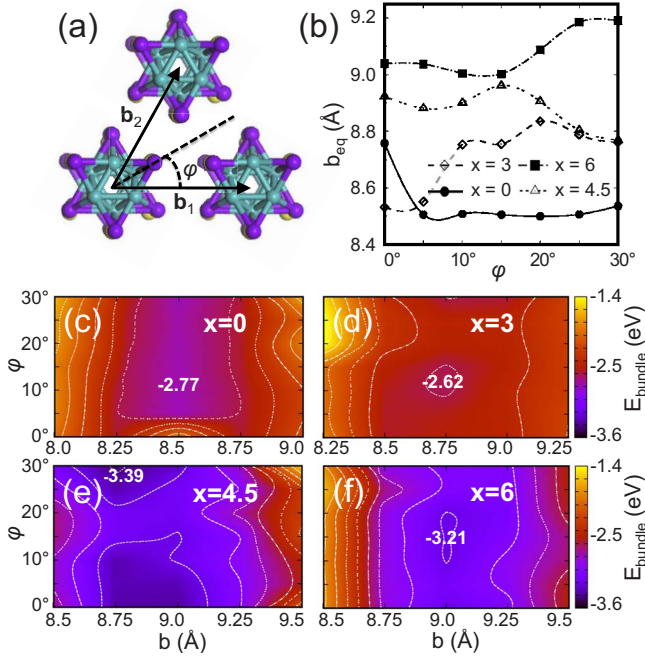


FIG. 2. (Color online) Equilibrium packing of $\text{Mo}_6\text{S}_{9-x}\text{I}_x$ nanowires. (a) End-on view of the structural arrangement of $\text{Mo}_6\text{S}_{9-x}\text{I}_x$ nanowires on a triangular lattice with $b=|\mathbf{b}_1|=|\mathbf{b}_2|$. (b) Equilibrium lattice constant b_{eq} as function of the wire orientation φ in four different stoichiometries with the lattice constant a corresponding to the shortest optimum in the $E_b(a)$ curves in Fig. 1(b). Contour plots of the bundling energy E_{bundle} as a function of b and φ for (c) Mo_6S_9 ($a=10.2$ Å), (d) $\text{Mo}_6\text{S}_6\text{I}_3$ ($a=11.0$ Å), (e) $\text{Mo}_6\text{S}_{4.5}\text{I}_{4.5}$ ($a=11.0$ Å), and (f) $\text{Mo}_6\text{S}_3\text{I}_6$ ($a=11.0$ Å). The bundling energy is the difference between the binding energies E_b per formula unit of isolated and bundled nanowires. The equipotential lines are separated by 0.2 eV.

To describe isolated nanowires in a periodic lattice arrangement, we placed them on a tetragonal lattice with a large interwire distance $b=19.7$ Å, about three times the nanowire diameter, to suppress interwire interaction. We sampled the rather short Brillouin zone of these one-dimensional (1D) structures with six k points in order to represent adequately the Bloch wave functions for the momentum space integration. A $6 \times 6 \times 6$ k -point sampling was used for the densely packed nanowire bundles represented by three-dimensional nanowire arrays. In selected systems the convergence of the electronic structure was tested by a twice as dense k -point grid. The charge density and potentials were determined on a real-space grid with a mesh cutoff energy of 150 Ry, which was sufficient to achieve a total-energy convergence of better than 2 meV/atom. We used a confinement energy shift of 0.01 Ry, which defines the cutoff radii of the atomic orbitals. All geometries were optimized without any symmetry constraints using the conjugate gradient method²⁵ until none of the residual Hellmann-Feynman forces acting on any atom would exceed 1.56×10^{-3} Ry/ a_B , where a_B is the Bohr radius. To probe the possibility of magnetic ordering in the nanostructures, we used the local-spin-density approximation (LSDA) as a systematic way to estimate the net magnetic moments and the amount of exchange splitting in the nanowires. Since LSDA calculations pertaining to mag-

netic ordering are generally less reliable than total-energy calculations, our results regarding magnetic properties are not as dependable as predicted electronic and structural data.

III. RESULTS

A. Structural arrangement in isolated nanowires

The atomic arrangement within an isolated $\text{Mo}_6\text{S}_{9-x}\text{I}_x$ nanowire is shown schematically in Fig. 1(a). The unit cell contains two Mo_6 octahedra decorated by S and I atoms, linked by stable S_3 linkages to an infinite chain. The two Mo_6 octahedra in the unit cell have the same structure with C_3 symmetry but are rotated by 180° with respect to each other. This atomic arrangement agrees with experimental data,¹⁴ including the presence of S_3 linkages that have been found more stable than I_3 linkages.⁹

Each of the Mo_6 octahedra in $\text{Mo}_6\text{S}_{9-x}\text{I}_x$ is decorated by the remaining $6-x$ sulfur and x iodine atoms, which occupy the sites denoted by A_i and B_i on each octahedron with $i=1, \dots, 6$. All decorating sites A_i and B_i are occupied by sulfur for $x=0$ and by iodine for $x=6$. Consequently, we should not expect any compositional disorder in Mo_6S_9 ($x=0$) and $\text{Mo}_6\text{S}_3\text{I}_6$ ($x=6$, the “636” structure). Several structural arrangements are possible in the intermediate iodine concentrations range $0 < x < 6$ with S and I coexisting on the Mo clusters. For $\text{Mo}_6\text{S}_6\text{I}_3$ ($x=3$, the “663” structure) we considered the stable arrangement of iodine atoms⁹ occupying A_i and B_i sites with $i=2, 4, 6$. For $\text{Mo}_6\text{S}_{4.5}\text{I}_{4.5}$ ($x=4.5$, the “644” structure) we considered the stable arrangement of iodine atoms⁷ occupying all six A_i sites and B_i sites with $i=1, 2, 5$. Since the stability of different structural arrangements with same composition was found to be similar in isolated $\text{Mo}_6\text{S}_{9-x}\text{I}_x$ nanowires,⁹ we may expect compositional disorder to occur for stoichiometries in the range $0 < x < 6$.

To make sure that the geometrical arrangements for each system correspond to true optima, we considered for each stoichiometry several initial geometries generated by subjecting uniformly expanded or compressed nanowires to random distortions or geometries based on semiempirical force fields. We considered a structure to represent the optimum geometry when the same structural arrangement was achieved starting from different geometries. We found it easier to distinguish between the functionality of decorating and linkage atoms in iodine-rich systems with $x \leq 6$, where $E_b(a)$ more clearly displays multiple minima with a similar binding energy according to Fig. 1(b).

Our results for the binding energy E_b of $\text{Mo}_6\text{S}_{9-x}\text{I}_x$ with respect to isolated atoms as a function of the lattice constant a are summarized in Fig. 1(b) for four different stoichiometries. Ignoring differences between elements in the 30-atom unit cell, the average binding energy per atom ranges between 4.8 and 5.8 eV, depending on composition, reflecting an unusually high stability of these compounds.⁹

A unique feature displayed by many $\text{Mo}_6\text{S}_{9-x}\text{I}_x$ compounds is the presence of multiple minima in the $E_b(a)$ relationship, seen in Fig. 1(b). The origin of these minima has been traced back to the presence of bistable S_3 linkages connecting chain segments.⁷ The bistability of the sulfur linkage bond originates in two similarly stable configurations, one

with a sharp and the other with an obtuse Mo-S-Mo bond angle,^{7,9} and occurs also in isolated sulfur chains.²⁶ The presence of two S_3 linkages per unit cell explains the presence of three minima in $E_b(a)$, associated with “short-short,” “short-long” or “long-short,” and “long-long” linkage configurations.

We found that inclusion of Mo $5p$ orbitals provided a net stabilization of the system but caused only very small changes in the optimum geometry. Our LSDA results indicate the occurrence of magnetic ordering for selected geometries, which causes additional stabilization of the systems.

B. Structural arrangement in nanowire bundles

Even though isolated $Mo_6S_{9-x}I_x$ nanowires are very stable, they may still benefit from additional stabilization when forming bundles.²⁷ We investigated interwire interactions for different stoichiometries in periodic nanowire lattices representing large bundles and present results in Fig. 2.

We found that the triangular lattice, spanned by the lattice vectors \mathbf{b}_1 and \mathbf{b}_2 and shown in Fig. 2(a), is the most stable arrangement or axially aligned nanowires with an approximate sixfold symmetry. The unit cell of this system is defined by the interwire distance $b=|\mathbf{b}_1|=|\mathbf{b}_2|$ and the axial lattice constant a . The orientation of the nanowire within the unit cell is described by the angle φ . Of the three structural minima in the $E_b(a)$ curve in Fig. 1(a), we focus in this publication only on the short-short isomer with $a \approx 11 \text{ \AA}$.

Due to the high symmetry of the structure, all information about the angular dependence of total-energy changes is contained in the interval $0^\circ \leq \varphi \leq 30^\circ$. In the following, we discuss the bundling energy E_{bundle} , defined as the difference between the binding energy per formula unit of relaxed isolated and bundled nanowires.

In Fig. 2(b) we display results for the equilibrium interwire distance b_{eq} as a function of the nanowire orientation φ . We find that the optimum interwire separation places atoms in neighboring nanowires at a distance, where orbital overlap cannot be neglected. As a general trend, the optimum interwire separation increases with increasing iodine concentration, since the atomic radius of the heavier iodine is larger than that of sulfur. We find only a weak dependence of b_{eq} on the orientation, with variations of $\leq 0.2 \text{ \AA}$, suggesting that the interwire interaction is not purely of van der Waals type. In that case, the electronic structure of bundles should weakly depend on the nanowire orientation and differ from isolated nanowires.

To get a better insight into the nature of interwire interactions, we present contour plots of the bundling energy as a function of the wire separation d and orientation φ in Figs. 2(c)–2(f) for four different stoichiometries. With a possible exception of $x=0$ in Fig. 2(c) and $x=4.5$ in Fig. 2(e), we found the interwire interaction to be rather isotropic and soft, as the total energy per unit cell changes by $\leq 0.2 \text{ eV}$ in a 0.5 \AA interval around the optimum interwire separation b_{eq} . For all compositions we found a bundling energy of roughly 3 eV per 30-atom unit cell, which translates to about 0.1 eV per atom or per 0.3-\AA -long nanowire segment. This is about twice as much as in $Mo_6S_4I_2$ nanowires with a different

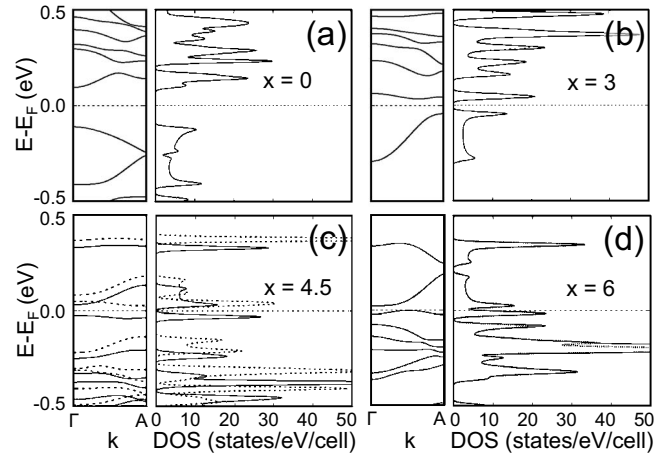


FIG. 3. Electronic band structure $E(k)$ along the axial direction Γ -A and the corresponding DOS of isolated $Mo_6S_{9-x}I_x$ nanowires with the lattice constant a corresponding to the shortest optimum in the $E_b(a)$ curves in Fig. 1(b). Results are presented for (a) Mo_6S_9 ($a=10.2 \text{ \AA}$), (b) $Mo_6S_6I_3$ ($a=11.0 \text{ \AA}$), (c) $Mo_6S_{4.5}I_{4.5}$ ($a=11.0 \text{ \AA}$), and (d) $Mo_6S_3I_6$ ($a=11.0 \text{ \AA}$). The densities of states have been convoluted with 0.02 eV wide Gaussians.

structure,⁹ suggesting that $Mo_6S_{9-x}I_x$ nanowires should form rather robust bundles that are not easy to separate.

C. Electronic structure of isolated nanowires

Presence of S_3 end groups, known to form stable “alligator clips” with preferential bonding and ideal contact to Au surfaces, suggests a possible application of $Mo_6S_{9-x}I_x$ nanowires in molecular electronics.^{7,9} We explored this possibility by studying the electronic structure of nanowires with four different stoichiometries and present the electronic band structure $E(k)$ as well as the density of states (DOS) of these systems in Fig. 3. The primary effect of a changing composition is to change the number of valence electrons per unit cell, which determine the Fermi level. We find that the changing orbital hybridization, causing structural relaxations, is at least equally important in its effect on the electronic structure.

As seen in Figs. 3(a) and 3(b), isolated $Mo_6S_{9-x}I_x$ nanowires with $x=0$ and $x=3$ are semiconducting. According to Fig. 3(d), the isolated $Mo_6S_3I_6$ nanowire exhibits a very narrow band gap at E_F that is suppressed by the convolution used in the density of states. Any amount of disorder should fill in states at E_F , turning the system into a poor metal. A flat band at E_F gives rise to a sharp peak in the density of states of $Mo_6S_{4.5}I_{4.5}$, shown in Fig. 3(c), causing a magnetic instability.⁷ Our LSDA calculations indicate that the system acquires a net magnetic moment of $1.0 \mu_B$ per unit cell while opening a 75 meV wide gap at E_F , turning into a magnetic semiconductor.⁷ Even though ferromagnetic ordering should not persist in these 1D systems at finite temperatures, we still may expect occurrence of magnetism in finite segments of $Mo_6S_{4.5}I_{4.5}$.

D. Electronic structure of nanowire bundles

To better understand the effect of bundle formation on the electronic structure, we displayed the band structure, density

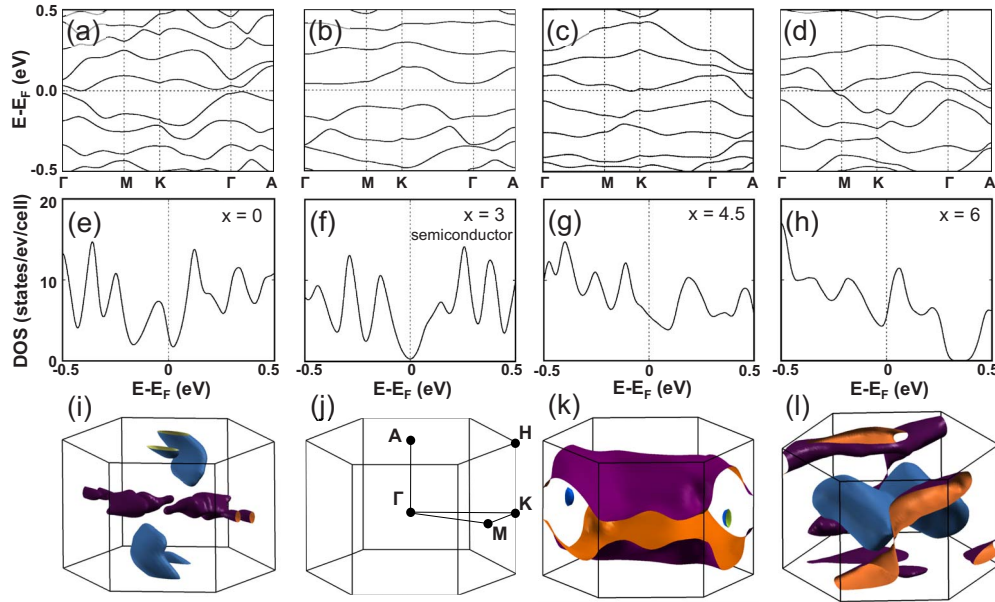


FIG. 4. (Color online) [(a)–(d)] Electronic band structure $E(k)$, [(e)–(h)] the corresponding DOS, and [(i)–(l)] the Fermi surface of bundled $\text{Mo}_6\text{S}_{9-x}\text{I}_x$ nanowires with the lattice constant a corresponding to the shortest optimum in the $E_b(a)$ curves in Fig. 1(b). Results for $x=0$ with $a=10.2$ Å and $x=3, 4.5, 6$ with $a=11.0$ Å are displayed in columns. The densities of states have been convoluted with 0.02 eV wide Gaussians. Since $\text{Mo}_6\text{S}_6\text{I}_3$ is a semiconductor and does not have a Fermi surface, we depict the empty Brillouin zone and the high-symmetry points in (j).

of states, and Fermi surface of $\text{Mo}_6\text{S}_{9-x}\text{I}_x$ nanowire arrays with $x=0, 3, 4.5, 6$ in Fig. 4. In absence of any interwire interaction, we would expect all bands to be flat along the Γ -M-K- Γ path in the Brillouin zone shown in Fig. 4(j). Also, in this case, the Γ -A band dispersion along the wire axis should be equal to that in Fig. 3 for isolated nanowires. Neither statement applies, as seen in the band structures displayed in Figs. 4(a)–4(d), reflecting presence of the interwire interaction discussed in Sec. III B.

As discussed in Sec. III C and seen in Fig. 3, isolated $\text{Mo}_6\text{S}_{9-x}\text{I}_x$ nanowires with $x=0, 3, 4.5, 6$ are semiconductors. This changes significantly due to the modified band dispersion in bundles. As seen in Figs. 4(a)–4(d) displaying the band structure and Figs. 4(e)–4(h) showing the density of states, only the system with the $x=3$ stoichiometry remains semiconducting whereas the other systems with $x=0, 4.5, 6$ either remain or turn metallic. None of the nanowire bundles is magnetic according to our LSDA calculations. This applies, in particular, to the $x=4.5$ stoichiometry, where a magnetic moment $1.0 \mu_B$ per unit cell at $a=11.0$ Å has been found in the isolated nanowire. The electronic density of states of bundled $\text{Mo}_6\text{S}_{4.5}\text{I}_{4.5}$ nanowires, shown in Fig. 4(g), no longer exhibits a sharp peak at the Fermi level, thus explaining the suppression of the magnetic instability according to Stoner criterion.

The Fermi surface of the metallic systems is depicted in Fig. 4(i) for $x=0$, Fig. 4(k) for $x=4.5$, and Fig. 4(l) for $x=6$. Our results indicate that Fermi surface states are distributed throughout the Brillouin zone. Whereas dependence of the interwire interaction on the wire orientation was found to be rather weak in Fig. 2, we did find important changes in the shape of the Fermi surface with changing φ . Our results for $x=4.5$ in Figs. 4(c), 4(g), and 4(k), obtained at $\varphi=30^\circ$,

indicate presence of states along the Γ -A line at E_F . For the $\varphi \approx 0^\circ$ wire orientation, there are no states along the Γ -A line at E_F . There are small differences in the density of states between both structures, and the $\varphi \approx 0^\circ$ system displays a hole in the Fermi surface around the Γ -A line.

To obtain a better insight into the onset of magnetism in $\text{Mo}_6\text{S}_{4.5}\text{I}_{4.5}$ ($x=4.5$) nanowires, we investigated the electronic structure of this system in more detail and present our results in Figs. 5 and 6. Our spin-polarized $E(k)$ data in Fig. 5 show the evolution of the band structure with changing interwire distance. For the sake of fair comparison, each structure was individually relaxed, starting with the $\varphi=0^\circ$ orientation of the nanowire array at $b=20$ Å and propagating this geometry during gradual reduction in the interwire distance. These results show the occurrence of a magnetic instability at large interwire separations, when the band associated with the frontier states flattens enough to yield a sharp peak in the density of states at E_F .

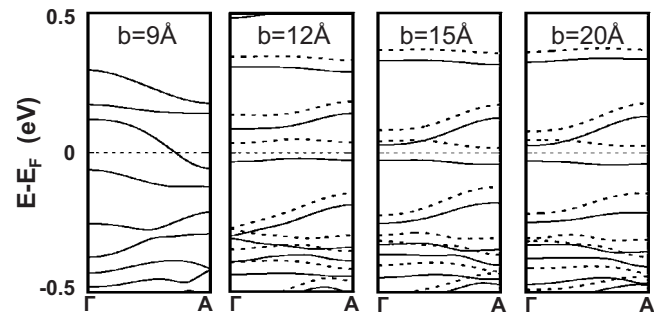


FIG. 5. Electronic band structure $E_1(k), E_2(k)$ of $\text{Mo}_6\text{S}_{4.5}\text{I}_{4.5}$ nanowire bundles with $a=11.0$ Å at interwire separations $9 \leq b \leq 20$ Å. The spin-resolved bands are represented by the solid and dashed lines.

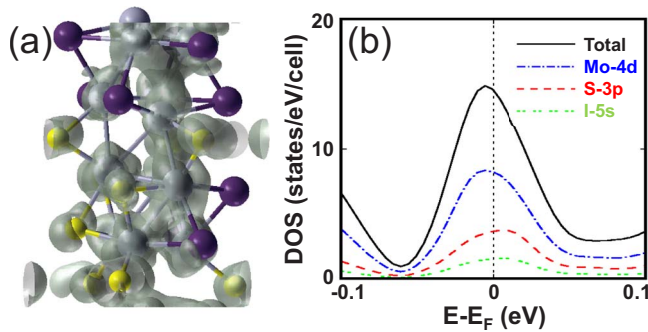


FIG. 6. (Color online) Nature of frontier states in $\text{Mo}_6\text{S}_{4.5}\text{I}_{4.5}$ nanowire bundles with $a=11.0$ Å at the equilibrium interwire separations $b=8.85$ Å and $\varphi \approx 0^\circ$. (a) Spatial distribution of states in the range $E_F-0.1$ eV $\leq E \leq E_F+0.1$ eV in the optimized bundle. The associated charge density is presented as the value $\rho=5 \times 10^{-4}$ e/Å³ along with the structural model. (b) Orbital-decomposed density of states in the same energy range around E_F .

In Fig. 6(a) we display the spatial distribution of states close to the Fermi level in the $\text{Mo}_6\text{S}_{4.5}\text{I}_{4.5}$ ($x=4.5$) nanowire bundle at the equilibrium interwire separation of 8.85 Å and $\varphi \approx 0^\circ$. Since the states are distributed rather uniformly along the nanowire and since, according to Fig. 6(b), the density of states at E_F is nonzero, we should expect corresponding nanowire bundles to behave as metallic quantum conductors that are sensitive to disorder and changes in the interwire distance. Decomposition of the electronic density of states in the same energy range $E_F-0.1$ eV $\leq E \leq E_F+0.1$ eV, shown in Fig. 6(b), indicates that the frontier states responsible for the magnetic instability have a predominant Mo 4d character with significant contributions from S 3p and I 5s states.⁷

IV. SUMMARY AND CONCLUSIONS

In summary, we used *ab initio* density-functional theory calculations to determine the effect of bundling on the equilibrium structure, electronic, and magnetic properties of $\text{Mo}_6\text{S}_{9-x}\text{I}_x$ nanowires with $x=0,3,4.5,6$. Each unit cell of these systems contains two S- and I-decorated Mo_6 clusters that are connected by S_3 linkages to form an ordered linear array. Due to the bistability of the sulfur linkages, the total energy of the nanowires exhibits typically many minima as a function of the wire length. We found the optimum interwire distance to depend primarily on composition and to a smaller degree on the orientation of the wires. Structural order is expected in bundles with $x=0$ and $x=6$, since there is no disorder in the decoration of the Mo clusters. We expect structural disorder in terms of the exact location of I and S atoms on Mo_6 octahedra and the interwire separation to occur in bundles with other stoichiometries. We found that the electronic structure of some nanowires can switch from metallic to semiconducting by changing the interwire separation. Also, we found that selected stable or metastable nanowire geometries exhibit ferromagnetic behavior. We expect that this type of nanowires may find a use as components of electronic devices in the near future.

ACKNOWLEDGMENTS

We thank Sora Park and Teng Yang for useful discussions. D.T. was partly supported by Kyung Hee University and the National Science Foundation under Cooperative Agreement No. EEC-0832785, titled “NSEC: Center for High-rate Nanomanufacturing.” Y.K. was partly supported by the NRF of Korea under Grant No. KRF-2010-0015656.

*Email: ykkwon@khu.ac.kr

†Email: tomanek@pa.msu.edu

¹M. Remskar, A. Mrzel, Z. Skraba, A. Jesih, M. Ceh, J. Demsar, P. Stadelman, F. Levy, and D. Mihailovic, *Science* **292**, 479 (2001).

²D. Vrbanić, M. Remskar, A. Jesih, A. Mrzel, P. Umek, M. Ponikvar, B. Jančar, A. Meden, B. Novosel, S. Pejovnik, P. Venturini, J. C. Coleman, and D. Mihailović, *Nanotechnology* **15**, 635 (2004).

³A. Kis, D. Mihailovic, M. Remskar, A. Mrzel, A. Jesih, I. Pionowski, A. J. Kulik, W. Benoit, and L. Forro, *Adv. Mater.* **15**, 733 (2003).

⁴I. Vilfan and D. Mihailovic, *Phys. Rev. B* **74**, 235411 (2006).

⁵A. Kis, G. Csanyi, D. Vrbanic, A. Mrzel, D. Mihailovic, A. Kulik, and L. Forro, *Small* **3**, 1544 (2007).

⁶B. Berčić, U. Pirnat, P. Kusar, D. Dvorsek, D. Mihailovic, D. Vengust, and B. Podobnik, *Appl. Phys. Lett.* **88**, 173103 (2006).

⁷T. Yang, S. Okano, S. Berber, and D. Tománek, *Phys. Rev. Lett.* **96**, 125502 (2006).

⁸I. Popov, T. Yang, S. Berber, G. Seifert, and D. Tománek, *Phys. Rev. Lett.* **99**, 085503 (2007).

⁹T. Yang, S. Berber, and D. Tománek, *Phys. Rev. B* **77**, 165426 (2008).

¹⁰L. Joly-Pottuz, F. Dassenoy, J. M. Martin, D. Vrbanic, A. Mrzel, D. Mihailovic, W. Vogel, and G. Montagnac, *Tribol. Lett.* **18**, 385 (2005).

¹¹F. Dassenoy, L. Joly-Pottuz, J. M. Martin, D. Vrbanic, A. Mrzel, D. Mihailovic, W. Vogel, and G. Montagnac, *J. Eur. Ceram. Soc.* **27**, 915 (2007).

¹²A. Meden, A. Kodre, J. Gomilsek, I. Arcon, I. Vilfan, D. Vrbanic, A. Mrzel, and D. Mihailovic, *Nanotechnology* **16**, 1578 (2005).

¹³M. Uplaznik, B. Bercic, J. Strle, M. I. Ploscaru, D. Dvorsek, P. Kusar, M. Devetak, D. Vengust, B. Podobnik, and D. D. Mihailovic, *Nanotechnology* **17**, 5142 (2006).

¹⁴V. Nicolosi, P. D. Nellist, S. Sanvito, E. C. Cosgriff, S. Krishnamurthy, W. J. Blau, M. L. H. Green, D. Vengust, D. Dvorsek, D. Mihailovic, G. Compagnini, J. Sloan, V. Stolojan, J. D. Carey, S. J. Pennycook, and J. N. Coleman, *Adv. Mater.* **19**, 543 (2007).

¹⁵D. Vrbanic, A. Meden, B. Novosel, S. Pejovnik, P. Umek, M. Ponikvar, and D. Mihailovic, *J. Nanosci. Nanotechnol.* **7**, 982 (2007).

¹⁶D. Mandrino, D. Vrbanic, M. Jenko, D. Mihailovic, and S. Pejovnik, *Surf. Interface Anal.* **40**, 1289 (2008).

¹⁷M. Rangus, M. Remskar, and A. Mrzel, *Microelectron. J.* **39**, 475 (2008).

- ¹⁸J. Andzane, J. Prikulis, D. Dvorsek, D. Mihailovic, and D. Erts, *Nanotechnology* **21**, 125706 (2010).
- ¹⁹M. Hummelgård, R. Zhang, T. Carlberg, D. Vengust, D. Dvorsek, D. Mihailovic, and H. Olin, *Nanotechnology* **21**, 165704 (2010).
- ²⁰J. P. Perdew and A. Zunger, *Phys. Rev. B* **23**, 5048 (1981).
- ²¹D. M. Ceperley and B. J. Alder, *Phys. Rev. Lett.* **45**, 566 (1980).
- ²²J. M. Soler, E. Artacho, J. D. Gale, A. García, J. Junquera, P. Ordejón, and D. Sánchez-Portal, *J. Phys.: Condens. Matter* **14**, 2745 (2002).
- ²³N. Troullier and J. L. Martins, *Phys. Rev. B* **43**, 1993 (1991).
- ²⁴L. Kleinman and D. M. Bylander, *Phys. Rev. Lett.* **48**, 1425 (1982).
- ²⁵M. R. Hestenes and E. Stiefel, *J. Res. Natl. Bur. Stand.* **49**, 409 (1952).
- ²⁶S. Okano and D. Tománek, *Phys. Rev. B* **75**, 195409 (2007).
- ²⁷S. H. Kang, Y. K. Kwon, and D. Tománek, *J. Phys.: Condens. Matter* (to be published)